
Conference or Workshop Item:
Koshuriyan, Zamir, Dowling, Ann and Karabasov, Sergey (2006) Comparison of Jet Noise Models. In: 12th AIAA-CEAS Aero-acoustics Conference, 08-10 May 2006.

Comparison of Jet Noise Models

Mohammed Z. Afsar*, Ann P. Dowling† and Sergey. A. Karabasov‡
University of Cambridge, Cambridge, CB2 1PZ, UK

Acoustic analogy theories for Jet Noise Prediction are formulated from the Navier Stokes equations using Green functions, describing wave propagation, and semi-empirical modeling of the turbulent statistics that act as noise sources. In a departure from this standpoint the Tam and Aurialt use an ad-hoc kinetic theory type argument that has been successful in predicting the 90 degree acoustic spectrum. In this paper we reassess the underlying assumptions of the Tam and Aurialt model. It is shown, while the Tam and Aurialt model can be interpreted as the integration of a source with a derivative of a Green function; the particular derivative is discontinuous across a thin shear layer, resulting in a sound power spectrum that is sensitive to the position of the discontinuity even when the acoustic wavelength is large. This is a disadvantage because there is some arbitrariness in the radial position of maximum shear, if a parallel shear flow is used to represent a developing jet. Comparison is made between predictions of the far-field sound from acoustic analogies and the Tam and Aurialt model.

I. Introduction

MANY theories for jet noise prediction are based upon an acoustic analogy. This is where the Navier-Stokes equations are recast as the linear fluctuations from a base flow, that describe the propagating waves, and the nonlinear fluctuations to represent the acoustic source terms. The original sound field problem can then be solved using a Green function solution, for the wave propagation, and a turbulence model describing the statistics of the source terms. Lighthill's original theory[1] described the acoustic propagation for a base flow at rest; since then, various analogies have been proposed. The Lilley equation[2] includes mean flow refraction effects in the propagation operator, by considering a parallel shear flow in the axial direction. Indeed, in the most general case the base flow would be an evolving mean flow that varies in all directions.

Acoustic analogies assume the source terms are known, and their statistics can be modeled in some manner. The source term in Lighthill's theory, T_{ij}, was given by an exact rearrangement of the Navier-Stokes equations, without explicit linearization of the flow variables. Hence, $T_{ij} = \rho v_i v_j + (p - \rho c_\infty^2)\delta ij - \tau_{ij}$; where, v_i is the fluid velocity, p is the pressure, ρ is the density and τ_{ij} the viscous stress tensor. Lighthill then assumed for the low Mach number cold jet, at least, the source term would be dominated by the self noise, or the so-called turbulence-turbulence interaction from correlated eddies. That is, $T_{ij} \approx \rho_\infty v_i' v_j'$, where now ρ_∞ is the density for the base flow at rest and v_i' is the fluctuating velocity. Although this neglected turbulence-shear interactions, or shear noise, the recent DNS analysis by Freund[3] for the Stromberg jet case[4] has shown the net acoustic power (all observation angles) from the self noise alone amounts to 83% of T_{ij} and is particularly dominant at higher observation angles, approaching 90 degrees.

Tam and Aurialt[5] introduced their model through a heuristic argument based on an analogy between the molecular pressure, from the kinetic theory of gases, and the turbulent pressure from packets of fine scale turbulence. The theoretical basis of their model initially seemed to be at odds with the acoustic analogy. It was later shown, however, by Morris and Farassat[6] that Tam and Aurialt's approach was equivalent to an acoustic analogy provided one represents the source and Green function consistently. Even though the difference to the acoustic analogy was simply an integration by parts, the Tam and Aurialt model had a convected time derivative on the source, rather than on the Green function in the form arising from Lilley's equation. Tam and Aurialt then modeled the convective derivative of the source term with Gaussian

*Ph.D. Research Student, Department of Engineering, Student Member AIAA.
†Professor, Department of Engineering, Member AIAA.
‡Research Fellow, Department of Engineering, Member AIAA.

statistics divided by the characteristic time scale, $\tau = \frac{k}{\epsilon}$; where, k is the turbulent kinetic energy, and ϵ the rate of energy dissipation. Several researchers[6,7] have pointed out this assumption would imply the Fourier transform of the source function becomes infinite as $\omega \to 0$, which is certainly not consistent with experimental data (ω is the frequency in rad/s). The acoustic spectrum using the Tam and Aurialt model leads to a frequency scaling on ω^2. This approach does remain in good agreement with the experimental data, for the higher observation angles, approaching 90 degrees. Goldstein[7] has suggested an alternative reason for the measured low frequency scaling: that it could be due to a source term in the energy equation.

In this paper we compare sound predictions using the Tam and Aurialt model and various acoustic analogies, for the Stromberg[4] test case: Reynolds number, 3600; Mach number, 0.9. The paper is organized as follows. In section 2, we develop the acoustic analogy formalism using Goldstein's[8] general set of linearized equations; with particular attention to the parallel shear layer and vortex sheet mean flows. We formulate a representation theorem using the adjoint Green function for a base flow defined by a general mean flow. We show, for a parallel shear layer, the adjoint equations can be written in a conservation form that does not involve derivatives of the mean flow profile. In section 3, we analyze these conservation equations numerically showing they are advantageous when the mean flow profile in defined on a discrete set of points. We then conclude in section 4, by discussing the predicted acoustic spectra using the Tam and Aurialt model in comparison with various acoustic analogies. We find the far-field pressure predicted by the Tam and Aurialt model is sensitive to slight changes in the mean flow profile. This arises because in their formulation the integrand is discontinuous across the shear layer, when the acoustic wavelength is large; resulting in sensitivity to the exact location of the source relative to the shear layer. That sensitivity does not arise in a formulation based on the acoustic analogy.

II. Acoustic Analogies

A. Governing Equations

Suppose an emanating jet flow contains a region of turbulence action that exists within the vicinity of the jet. Mathematically, the turbulence is represented by source functions defined within the region near the jet, and described by coordinates $(\mathbf{y}, \tau)$. The sources are assumed to be representative of the turbulent field, in the statistical sense, and are the generators of jet noise that propagates to the far field, at the observer position, $(\mathbf{x}, t)$.

We develop the usual acoustic analogy beginning with the Navier Stokes Equations; the noise generated by heat conduction and viscous dissipation is neglected.[1] The resulting Euler equations are re-written with the dependent variables expressed as the sum of their mean, and perturbation about that mean. Hence, the bar and single prime are the time average, and its perturbation; the tilde and double prime are the Favre average, and its perturbation. The averaging operations are defined in the usual manner:

$$\overline{(\bullet)} \equiv \lim_{T\to\infty} \int_{-T}^{T} (\bullet)(\mathbf{y},\tau)d\tau \quad \text{and} \quad \bar{\rho}\widetilde{(\bullet)} \equiv \overline{\rho(\bullet)}. \tag{1}$$

The application of the averaging definitions linearizes Euler equations about a base flow with density $\bar{\rho}$, pressure $\bar{p}$, and velocity $\tilde{v}_j$. We use the simplified version proposed by Goldstein,[8] which casts the system of equations as the linearized Euler operator, on the left hand side, and simple non-linear source terms, on the right hand side.

$$\frac{\partial \rho'}{\partial \tau} + \frac{\partial}{\partial y_j}(\rho' \tilde{v}_j + u_j) = 0 \tag{2}$$

$$\frac{\partial u_i}{\partial \tau} + \frac{\partial}{\partial y_j}(\tilde{v}_j u_i) + \frac{\partial p'}{\partial y_i} + u_j \frac{\partial \tilde{v}_i}{\partial y_j} - \left(\frac{\rho'}{\bar{\rho}}\right)\frac{\partial \tilde{\tau}_{ij}}{\partial y_j} = \frac{\partial T'_{ij}}{\partial y_j} \quad i = 1,..3. \tag{3}$$

$$\left(\frac{1}{\gamma-1}\right)\frac{\partial p'}{\partial \tau} + \left(\frac{1}{\gamma-1}\right)\frac{\partial}{\partial y_j}(p'\tilde{v}_j) + \frac{\partial}{\partial y_j}(u_j \tilde{h}) + p'\frac{\partial \tilde{v}_j}{\partial y_j} - \left(\frac{u_i}{\bar{\rho}}\right)\frac{\partial \tilde{\tau}_{ij}}{\partial y_j} = Q \tag{4}$$

The momentum variable is defined with zero time average, $u_i = \rho v_i''$; and summation applies across repeated indices. In this system, the Favre averaged stagnation enthalpy and its perturbation are defined, i.e.:

$$\tilde{h}_o = \tilde{h} + \frac{1}{2}\tilde{v}^2 \quad \text{and} \quad h_o'' = h'' + \tilde{v}_i v_i'' + \frac{1}{2}v''^2 \tag{5}$$

The source terms, on the right hand side of the linearized equations, are given by:

$$T'_{ij} = -(\rho v_i'' v_j'' - \widetilde{\bar{\rho} v_i'' v_j''}) \tag{6}$$

$$Q = \underbrace{-\tilde{v}_j \frac{\partial T'_{ij}}{\partial y_i} + \frac{1}{2}\delta_{ij}\left[\frac{DT'_{ij}}{D\tau} + \frac{\partial \tilde{v}_k}{\partial y_k} T'_{ij}\right]}_{T_{ij}\text{-mean flow interaction}} \underbrace{- \frac{\partial}{\partial y_j}\left(\rho v_j'' h_o'' - \widetilde{\bar{\rho} v_j'' h_o''}\right)}_{\text{Heat source}} \tag{7}$$

where, the convective derivative is defined as:

$$\frac{D}{D\tau} = \frac{\partial}{\partial \tau} + \tilde{v_j}\frac{\partial}{\partial y_j} \tag{8}$$

In this paper, we concentrate on propagation effects described through the Green function and so consider the effect of the source term T'_{ij}, in the momentum equation. The perturbations in density are neglected, i.e. $\rho(\mathbf{y}, \tau) \approx \bar{\rho}(\mathbf{y})$, compared to the fluctuations in velocity. Physically, for the cold jet, the density does not display significant fluctuation to include it within T'_{ij}. The mean density, $\bar{\rho}(\mathbf{y})$, however, can be a function of $\mathbf{y}$ for the wave propagation problem. In addition the effect of $\tilde{\tau}_{ij}$, where $\tilde{\tau}_{ij} = \delta_{ij}\bar{p} + \widetilde{\bar{\rho} v_i'' v_j''}$, is neglected in the propagation operator. It could, in principle, be included when considering a base flow determined by a CFD solution, but we do not expect its contribution to be significant.

B. Green Function Equations and Sound Field Representation Theorems

The wave propagation problem is solved in the frequency domain using the adjoint Green function method, because it allows specification of the source region for a particular observer point (Dowling et al,[9] Tam and Aurialt[10]). We solve the adjoint equations in the frequency domain from the outset, to avoid the instability waves the propagation operator may support (Agarwal *et al*[11]). In practical terms, the Green function method amounts to solving the homogeneous equations (i.e., when the right hand side is zero) in the jet region, and matching the solution to a time-harmonic sink in the far field, where the mean flow is zero. We use the following Fourier transform pair:

$$\hat{f}(\omega) = \int_{-\infty}^{\infty} f(\tau) e^{-i\omega\tau}\, d\tau \tag{9}$$

$$f(\tau) = \frac{1}{2\pi}\int_{-\infty}^{\infty} \hat{f}(\omega) e^{i\omega\tau}\, d\omega. \tag{10}$$

The representation theorem is then formulated in the usual manner. For example, by taking the momentum-like Green function and performing the inner product of this and the momentum equation, Eq. 3, gives the adjoint equation after integrating each term by parts and using the divergence theorem. Similarly for mass and energy; hence the representation theorem for pressure is given by:

$$\hat{p}(\mathbf{x}, \omega) = -\int_{V_\infty} \hat{G}_i(\mathbf{y}, \omega \mid \mathbf{x}) \frac{\partial \hat{T}_{ij}}{\partial y_j}(\mathbf{y}, \omega)\, d^3\mathbf{y} \tag{11}$$

where, $\hat{T}_{ij}(\mathbf{y}, \omega)$ is now the Fourier transform of $T'_{ij}(\mathbf{y}, \tau)$, and $\hat{\mathbf{G}}(\mathbf{y}, \omega \mid \mathbf{x})$, the Fourier transform of the adjoint Green's function, satisfies:

$$i\omega\hat{G}_o + \tilde{v}_j \frac{\partial \hat{G}_o}{\partial y_j} = 0 \tag{12}$$

$$i\omega\hat{G}_j + \frac{\partial \hat{G}_o}{\partial y_j} + \tilde{v}_i \frac{\partial \hat{G}_j}{\partial y_i} - \hat{G}_i \frac{\partial \tilde{v}_i}{\partial y_j} + \tilde{h} \frac{\partial \hat{G}_4}{\partial y_j} = 0 \quad j = 1, ..3. \tag{13}$$

$$\left(\frac{i\omega}{\gamma - 1}\right) \hat{G}_4 + \left(\frac{\tilde{v}_j}{\gamma - 1}\right) \frac{\partial \hat{G}_4}{\partial y_j} - \hat{G}_4 \frac{\partial \tilde{v}_j}{\partial y_j} + \frac{\partial \hat{G}_j}{\partial y_j} = \delta(\mathbf{y} - \mathbf{x}) \tag{14}$$

In this system, $\hat{G}_o$ represents the adjoint density-like variable; $\hat{G}_1$-$\hat{G}_3$ are the adjoint momentum-like variables and $\hat{G}_4$ is the variable in the adjoint energy equation, a pressure-like variable.

For the general case of an evolving jet, we are relying on a near field CFD solution for the mean flow profile. There may, however, be some numerical difficulty in computing the mean velocity derivatives when using CFD data that is known on a discrete set of points. In particular, at high frequencies where the acoustic resolution may need to be greater than the mean flow. But if the mean velocity dilatation is zero, i.e. $\nabla.\tilde{\mathbf{v}} = 0$, which applies to a parallel shear layer, then it is possible to redefine the adjoint system of equations in a conservation form that does not include derivatives of the mean flow. This easily follows by defining another Green function:

$$\hat{G}_5(\mathbf{y}, \omega \mid \mathbf{x}) = \frac{1}{\gamma - 1} \frac{D_1 \hat{G}_4}{D\tau}(\mathbf{y}, \omega \mid \mathbf{x}) \tag{15}$$

The convective derivative in the axial direction, $D_1/D\tau$, is understood to represent:

$$i\omega + U \frac{\partial}{\partial y_1} \tag{16}$$

Then Eq. (12) is unchanged and Eqs. (13) and (14) become:

$$\frac{1}{\tilde{c}^2} \frac{D_1^2 \hat{G}_j}{D\tau^2} + \frac{\partial \hat{G}_5}{\partial y_j} = 0 \tag{17}$$

$$\hat{G}_5 + \frac{\partial \hat{G}_j}{\partial y_j} = \delta(\mathbf{y} - \mathbf{x}) \tag{18}$$

where, by parallel shear layer we specifically mean:

$$\tilde{v}_j = \delta_{j1} U(y_2, y_3) \quad \bar{p} = p_\infty \quad \bar{\rho} = \bar{\rho}(y_2, y_3) \quad \tilde{h} = \tilde{h}(y_2, y_3) \tag{19}$$

The numerical convenience of Eqs. (17) and (18) is discussed later in §3. Indeed, another advantage of of Eqs. (17) and (18) is the absence of singular terms when the shear layer is very thin. Hence, the jump conditions across a thin shear layer follow immediately.

We adopt a cylindrically based coordinate system, for a jet flow that is circular cylindrical; hence $\mathbf{y} = (y_1, r, \psi)$ and $\mathbf{x} = (x_1, R, \Psi)$. The mean flow is directed axially in y_1, and a function of r; the observer is in the far field at an angle θ to the jet axis, i.e. $cos\theta = x_1/R$. In the limiting case, the thin shear layer tends to a vortex sheet mean flow, where the mean velocity is uniform in the jet region and discontinuous across the jet boundary. Integrating the adjoint energy equation, Eq. (18), over a infinitesimal disk of volume V_ϵ positioned across the jet boundary, with its inner surface at $a - \epsilon$ and outer radius $a + \epsilon$, shows:

$$\lim V_e \to 0 \int_{V_\epsilon} \left(\hat{G}_5(\mathbf{y}, \omega \mid \mathbf{x}) + \nabla.\hat{\mathbf{G}}(\mathbf{y}, \omega \mid \mathbf{x}) \right) dV_e = 0 \tag{20}$$

The assumption that $\hat{G}_5$ remains bounded implies its volume integral tends to zero as the shear layer thickness tends to zero. Application of the divergence theorem shows the normal component of $\hat{\mathbf{G}}$, i.e. $\hat{G}_r(\mathbf{y}, \omega \mid \mathbf{x})$, remains continuous. The adjoint momentum equation, Eq. (17), similarly shows that $\hat{G}_5$ is continuous. The jump condition for $d\hat{G}_5/dr$ can be expressed quite simply by taking Fourier transforms in y_1, writing

$\partial/\partial y_1 \rightarrow ik$, where, k is the wave number in the axial direction, and using Eq. (17). If we use our original variable $\hat{G}_4$ these jump conditions become:

$$\Big[(i\omega + Uik)\hat{G}_4(\mathbf{y},\omega \mid \mathbf{x})\Big]_{a-\epsilon}^{a+\epsilon} = 0 \tag{21}$$

$$\left[\frac{\tilde{h}}{(i\omega + Uik)}\frac{d}{dr}\hat{G}_4(\mathbf{y},\omega \mid \mathbf{x})\right]_{a-\epsilon}^{a+\epsilon} = 0 \tag{22}$$

where, $a \pm \epsilon$ refer to radii on either side of the jet interface. Eq. (21) then implies the Green function $\hat{G}_4$ is discontinuous across a thin shear layer, and the convective derivative of $\hat{G}_4$, i.e. $D_1\hat{G}_4/D\tau$, remains continuous.

C. Power Spectral Density and Correlation Function Representation

The power spectral density of the far-field pressure follows from Eq. (11). In the spirit of Lighthill, we isolate the source term, by integrating Eq. (11) by parts to place the derivatives onto the Green function, hence:

$$\mathbf{P}(\mathbf{x},\omega) = \int\limits_{V_\infty(\mathbf{y})}\int\limits_{V_\infty(\mathbf{\Delta})} \frac{\partial\hat{G}_j}{\partial y_i}(\mathbf{y},-\omega \mid \mathbf{x})\frac{\partial\hat{G}_l}{\partial y_k}(\mathbf{y}+\mathbf{\Delta},\omega \mid \mathbf{x})\mathbf{R_{ijkl}}(\mathbf{y},\mathbf{\Delta},\omega)\,d^3\mathbf{\Delta}\,d^3\mathbf{y} \tag{23}$$

The power spectral density, $\mathbf{P}(\mathbf{x},\omega)$, and the 4th rank cross power spectral density of the statistically stationary sources, $\mathbf{R_{ijkl}}(\mathbf{y},\mathbf{\Delta},\omega)$, are defined in the usual way:

$$\mathbf{P}(\mathbf{x},\omega) = \int\limits_{-\infty}^{\infty} \overline{p'(\mathbf{x},\tau)p'(\mathbf{x},\tau+\tau_0)}e^{-i\omega\tau_0}\,d\tau_0 \tag{24}$$

$$\mathbf{R_{ijkl}}(\mathbf{y},\mathbf{\Delta},\omega) = \int\limits_{-\infty}^{\infty} \overline{T'_{ij}(\mathbf{y},\tau)T'_{kl}(\mathbf{y}+\mathbf{\Delta},\tau+\tau_0)}e^{-i\omega\tau_0}\,d\tau_0 \tag{25}$$

We adopt the simplest kinematic representation for $\mathbf{R_{ijkl}}$, viz.

$$\mathbf{R_{ijkl}}(\mathbf{y},\mathbf{\Delta},\omega) = \delta_{ij}\delta_{kl}Q_s(\mathbf{y},\mathbf{\Delta},\omega) \tag{26}$$

where, $Q_s(\mathbf{y},\mathbf{\Delta},\omega)$ represents the two-point correlation function of $\frac{1}{3}\hat{T}_{nn}$ at $\mathbf{y}$ and $\mathbf{y}+\mathbf{\Delta}$; with δ_{ij}-δ_{kl} being unity tensors. The correlation function reduces to the statistical assessment of $\frac{1}{3}\bar{\rho}\overline{u''^2}$, where $\overline{u''^2}$ is the mean square amplitude of the velocity. The Green function products in the integrand of Eq. (23) simplify to:

$$\begin{aligned}\frac{\partial\hat{G}_j}{\partial y_i}(\mathbf{y},-\omega \mid \mathbf{x})\frac{\partial\hat{G}_l}{\partial y_k}(\mathbf{y}+\mathbf{\Delta},\omega \mid \mathbf{x})\delta_{ij}\delta_{kl}Q_s(\mathbf{y},\mathbf{\Delta},\omega) \\ = \frac{\partial\hat{G}_j}{\partial y_j}(\mathbf{y},-\omega \mid \mathbf{x})\frac{\partial\hat{G}_l}{\partial y_l}(\mathbf{y}+\mathbf{\Delta},\omega \mid \mathbf{x})Q_s(\mathbf{y},\mathbf{\Delta},\omega)\end{aligned} \tag{27}$$

The spatial derivatives, $\partial/\partial y_j$, on the right hand side of Eq. (27), are re-written using the adjoint energy equation, Eq. (14). For a parallel shear flow, Eq. (14) shows the divergence of the Green function $\hat{G}_j$ reduces to the convective derivative on $\hat{G}_4$,

$$\frac{\partial\hat{G}_j}{\partial y_j} \sim -\frac{1}{\gamma-1}\frac{D_1\hat{G}_4}{D\tau} \tag{28}$$

Therefore, using this relationship and Eq. (27) allows the power spectral density to be written in terms of $D_1\hat{G}_4/D\tau$:

$$\mathbf{P}(\mathbf{x},\omega) = \frac{1}{(\gamma-1)^2}\int\limits_{V_\infty(\mathbf{y})}\int\limits_{V_\infty(\mathbf{\Delta})} \frac{D_1\hat{G}_4}{D\tau}(\mathbf{y},-\omega \mid \mathbf{x})\frac{D_1\hat{G}_4}{D\tau}(\mathbf{y}+\mathbf{\Delta},\omega \mid \mathbf{x})Q_s(\mathbf{y},\mathbf{\Delta},\omega)\,d^3\mathbf{\Delta}\,d^3\mathbf{y} \tag{29}$$

which is equivalent to Eq. (61) in Morris and Farassat.[6] In this form $Q_s(\mathbf{y},\boldsymbol{\Delta},\omega)$ is represented by a model function. We use the Gaussian model given by Tam and Aurialt[5] where, U is the mean flow velocity and, $\hat{q}^2$ is proportional to $4/9ths$ of the mean square fluctuating kinetic energy; l_s is the characteristic length scale and τ_s is the characteristic time scale.

$$Q_s(\mathbf{y},\boldsymbol{\Delta},\omega) = \sqrt{\frac{\pi}{\ln 2}}\hat{q}^2\frac{l_s}{U}exp\left(-\frac{\mid \Delta_1 \mid}{U\tau_s} - \frac{ln2}{l_s^2}(\Delta_2^2+\Delta_3^2) - \frac{\omega^2 l_s^2}{4\bar{u}^2\ln 2} - \frac{i\omega\Delta_1}{U}\right) \tag{30}$$

In this paper, we assume the variation of the Green function over the correlation length in the 2 and 3 directions are small compared to the acoustic wavelength. For a parallel jet the dependence on Δ_1 is approximated, following Tam and Aurialt:[5]

$$\hat{G}_4(\mathbf{y}+\boldsymbol{\Delta},\omega \mid \mathbf{x}) \approx \hat{G}_4(\mathbf{y},\omega \mid \mathbf{x})e^{-i\frac{\omega}{c_\infty}\Delta_1 cos\theta} \tag{31}$$

for $\mathbf{x}$ in the far field. When the acoustic wavelength is the same order as the correlation lengths, Δ_2, Δ_3, or the jet is no longer parallel, the integral over $\boldsymbol{\Delta}$ in Eq. (29) then needs to be evaluated numerically. That analysis can be found in Karabasov and Hynes.[12] We focus on the approximated form when the Green function product conveniently reduces,

$$\frac{D_1\hat{G}_4}{D\tau}(\mathbf{y},-\omega \mid \mathbf{x})\frac{D_1\hat{G}_4}{D\tau}(\mathbf{y}+\boldsymbol{\Delta},\omega \mid \mathbf{x}) = \left|\frac{D_1\hat{G}_4}{D\tau}(\mathbf{y},\omega \mid \mathbf{x})\right|^2 e^{-i\frac{\omega}{c_\infty}\Delta_1 cos\theta} \tag{32}$$

The power spectral density equation then further simplifies,

$$\mathbf{P}(\mathbf{x},\omega) = \frac{1}{(\gamma-1)^2}\int\limits_{V_\infty(\mathbf{y})}\left|\frac{D_1\hat{G}_4}{D\tau}(\mathbf{y},\omega \mid \mathbf{x})\right|^2 \int\limits_{V_\infty(\boldsymbol{\Delta})} Q_s(\mathbf{y},\boldsymbol{\Delta},\omega)e^{-i\frac{\omega}{c_\infty}\Delta_1 cos\theta}\, d^3\boldsymbol{\Delta}\, d^3\mathbf{y} \tag{33}$$

The intervening steps, detailing the integration in $\boldsymbol{\Delta}$, have been spelled out by Tam and Aurialt;[5] our principal interest is in the behavior of the integrand of $\mathbf{P}(\mathbf{x},\omega)$ in $V_\infty(\mathbf{y})$. The final form of power spectral density then follows as,

$$\mathbf{P}(\mathbf{x},\omega) = \frac{1}{(\gamma-1)^2}\int\limits_{V_\infty(\mathbf{y})}\left|\frac{D_1\hat{G}_4}{D\tau}(\mathbf{y},\omega \mid \mathbf{x})\right|^2 q_s(\mathbf{y},\omega)\, d^3\mathbf{y} \tag{34}$$

where, the model form of $q_s(\mathbf{y},\omega)$ is then given by:

$$q_s(\mathbf{y},\omega) = 2\left(\frac{\pi}{\ln 2}\right)^{\frac{3}{2}}\hat{q}^2 l_s^3\tau_s exp\left(-\frac{\omega^2 l_s^2}{4\bar{u}^2\ln 2}\right)\frac{1}{1+\omega^2\tau_s^2\left(1-\frac{\bar{u}}{c_\infty}\cos\theta\right)^2} \tag{35}$$

and represents,

$$q_s(\mathbf{y},\omega) = \int\limits_{\boldsymbol{\Delta}} Q_s(\mathbf{y},\boldsymbol{\Delta},\omega)e^{-i\frac{\omega}{c_\infty}\Delta_1 cos\theta}\, d^3\boldsymbol{\Delta} \tag{36}$$

In this model the statistical quantities $(\hat{q}, l_s, \tau_s)$ are scaled on the local values of the turbulent kinetic energy, k, and the rate of energy dissipation, ϵ. They are defined as,

$$\hat{q}^2 = \frac{4}{9}\bar{\rho}^2A^2k^2, \quad l_s = c_l\frac{k^{\frac{3}{2}}}{\epsilon}, \quad \text{and} \quad \tau_s = c_\tau\frac{k}{\epsilon} \tag{37}$$

The empirical constants, (A, c_l, c_τ) are chosen for best fit to the experimental data. In this study, we obtain the $(\hat{q}, l_s, \tau_s)$ and the mean flow from a RANS solution.

D. Comparison to the Tam and Aurialt Model

Consider now the mathematical difference between a representation theorem based on the acoustic analogy, as in Eq. (34), and the Tam and Aurialt model.[5] Morris and Farassat[6] have shown the Tam and Aurialt model does indeed correspond to an acoustic analogy if the source is modeled consistently. In our notation, the Tam and Aurialt model follows by integrating Eq. (29) by parts to transfer the convective derivative onto the source term. The resulting power spectral density involves the integration of the Green function $\hat{G}_4$ at locations $\mathbf{y}$ and $\mathbf{y}+\mathbf{\Delta}$; and the two point correlation of $D_1 T_{ij}/D\tau$, modeled by the Gaussian statistics, given by Eq. (30), divided by the characteristic time scale squared, τ_s^2. After the Green function approximation is applied, and integrations in $\mathbf{\Delta}$ performed, the power spectral density using the Tam and Aurialt approach is:

$$\mathbf{P}(\mathbf{x},\omega) = \frac{1}{(\gamma-1)^2} \int\limits_{V_\infty(\mathbf{y})} \mid \hat{G}_4(\mathbf{y},\omega \mid \mathbf{x}) \mid^2 \frac{q_s(\mathbf{y},\omega)}{\tau_s^2}\, d^3\mathbf{y} \tag{38}$$

where, $q_s(\mathbf{y},\omega)$ is given by Eq. (35).

The analysis of the limiting form of the Green functions has shown $D_1\hat{G}_4/D\tau$ remains continuous across a thin shear layer, whereas $\hat{G}_4$ is discontinuous. Therefore, the integrand in Eq. (38) is also discontinuous across a thin shear layer, because it uses $\hat{G}_4$ in its representation theorem and models the convective derivative of the source term as a continuous function.

Practically speaking, if one is using a parallel shear flow to represent an evolving jet there will be some arbitrariness in the radial position of maximum shear relative to the source. Sound predictions obtained using Eq. (34) are independent of slight differences in the location of the shear layer. The same is not true for Eq. (38), which the Tam and Aurialt model uses, because the integrand can have discontinuous behavior. We analyze this numerically in §4.

III. Numerical Analysis of Adjoint Green Functions

In this section we solve the adjoint equations numerically using a mean flow defined derived from a CFD solution and hence on a discrete set of points. We focus on the parallel shear layer, comparing the numerical solutions from an explicit second order equation in $\hat{G}_4$, and Eqs. (17)-(18) that avoid mean flow derivatives altogether.

A. Second Order Equation

A standard way to determine $\hat{G}_4$, the adjoint pressure-like Green function, in a parallel shear flow, is to formulate an explicit Green function equation. This single equation in $\hat{G}_4$ follows by eliminating $\hat{G}_j$ from the adjoint Eqs. (12)-(14), after the application of the parallel shear flow conditions given by Eq. (19). Therefore,

$$-\frac{D_1}{D\tau}\left[\frac{D_1^3}{D\tau^3} - \frac{\partial^2}{\partial y_j^2}\left(\tilde{c}^2\frac{D_1}{D\tau}\right) + \frac{\partial}{\partial r}\left(\frac{d\tilde{c}^2}{dr}\frac{D_1}{D\tau}\right)\right]\hat{G}_4 + 2\frac{dU}{dr}\tilde{c}^2\frac{\partial^2}{\partial y_1 \partial r}\frac{D_1}{D\tau}\hat{G}_4 = (\gamma-1)\frac{D_1^3}{D\tau^3}\delta(\mathbf{y}-\mathbf{x}) \tag{39}$$

The usual adjoint Lilley equation, defined by the Green function $\hat{G}_a$, and appearing as Eq. (5) in Tam and Aurialt,[10] is related to $\hat{G}_4$ by the correspondence: $\hat{G}_4 = -(\gamma-1)D_1^2\hat{G}_a/D\tau^2$. To solve Eq. (39) we take Fourier transforms in the axial direction y_1, with wave number k, and in the azimuthal ψ, with the angular order m. This gives a second order equation in r,

$$\begin{aligned}&\frac{d^2G_4^\dagger(r)}{dr^2} + \left(\frac{1}{r} - \frac{1}{\bar{\rho}}\frac{d\bar{\rho}}{dr}\right)\frac{dG_4^\dagger(r)}{dr} \\ &+ \left[-\frac{\hat{k}}{\bar{D}_o}\frac{d\bar{M}}{dr}\frac{1}{\bar{\rho}}\frac{d\bar{\rho}}{dr} - \frac{2\hat{k}^2}{\bar{D}_o^2}\left(\frac{d\bar{M}}{dr}\right)^2 + \frac{\hat{k}}{\bar{D}_o}\frac{1}{r}\frac{d\bar{M}}{dr} + \frac{\hat{k}}{\bar{D}_o}\frac{d^2\bar{M}}{dr^2} - \frac{\omega^2}{c_\infty^2}\hat{k}^2 + \frac{\omega^2}{\tilde{c}^2}\bar{D}_o^2 - \frac{m^2}{r^2}\right]G_4^\dagger(r) = 0\end{aligned} \tag{40}$$

valid away from the observer position. $G_4^\dagger(r)$ is then solved by numerically integrating Eq. (40) and matching to the solution to the sink. The mean flow is defined by, $\bar{M}(r) = \frac{U(r)}{c_\infty}$; and $\bar{D}_o(r) = 1 + \bar{M}(r)\hat{k}$. The axial

wave number k is non-dimensionalised as, $\hat{k} = k(c_\infty/\omega)$; with the angular order being expanded as a Fourier series.

B. First Order System: Solution to Eqs. (17) & (18)

The solution to Eqs. (17) & (18) is found by taking the Fourier transforms in y_1 and ψ. This gives two equations for $G_5^\dagger(r)$ and $G_r^\dagger(r)$:

$$\frac{dG_5^\dagger(r)}{dr} = \left[\left(\frac{\omega}{\tilde{c}}\right)^2 \bar{D}_o^2\right] G_r^\dagger(r) \tag{41}$$

$$\frac{dG_r^\dagger(r)}{dr} = \left[\frac{\hat{k}^2}{\bar{D}_o^2}\left(\frac{\tilde{c}}{c_\infty}\right)^2 + \frac{\left(\frac{m}{r}\right)^2}{\left(\frac{\omega}{\tilde{c}}\right)^2 \bar{D}_o^2} - 1\right] G_5^\dagger(r) - \frac{G_r^\dagger(r)}{r} \tag{42}$$

The key feature of this system is the elimination of all mean flow derivatives. The coefficients of (41) & (42) depend on the mean flow only.

C. Comparison of Numerical Solutions

In this study we allow the Green functions to be weakly causal, which satisfy boundedness conditions at infinity, when $\mid \mathbf{y}, \tau \mid \rightarrow \infty$ (Dowling *et al*) .[9] We use the method of stationary phase to evaluate the inverse Fourier transform in axial wavenumber, k, by deforming the integration contour along path of steepest descent; hence in (40), (41) and (42) $\hat{k} = -cos\theta$. The ordinary differential Eqs. (40), (41) & (42) are solved numerically, using a variable step 4th order Runge Kutta scheme. The integration begins by assuming the solution is bounded algebraically at $r = 0$, as r^m, where r is starting value. Therefore, we can express the Green function solution in the jet region, after making the usual far field approximation, $\mid \mathbf{x} - \mathbf{y} \mid \approx \mid \mathbf{x} \mid$ when $\mathbf{x} \rightarrow \infty$,

$$\hat{G}_4(y_1, r, \psi, \omega \mid R_o) = \frac{i(\gamma-1)\omega}{4\pi \mid \mathbf{x} \mid c_\infty^2} e^{-i\frac{\omega}{c_\infty}(y_1 \cos\theta - \mid \mathbf{x} \mid)} \sum_{m=0}^{\infty} \epsilon_m (-i)^m A_m(\omega, \theta) G_4^\dagger(r) \tag{43}$$

where, $\epsilon = 1$ if $m = 0$ and $\epsilon = 2$ if $m \geq 1$; for integral m.

In the far field the mean flow is zero, the Green function solution to a sink then follows immediately. For example in terms of $\hat{G}_4$:

$$\hat{G}_{4_{SINK}} = \frac{i(\gamma-1)\omega}{4\pi \mid \mathbf{x} \mid c_\infty^2} e^{-i\frac{\omega}{c_\infty}(y_1 \cos\theta - \mid \mathbf{x} \mid)} \sum_{m=0}^{\infty} \epsilon_m (-i)^m \left[J_m\left(\frac{\omega \sin\theta}{c_\infty} R_o\right) + B_m(\omega, \theta) H_m^{(1)}\left(\frac{\omega \sin\theta}{c_\infty} R_o\right)\right] \tag{44}$$

where, J_m is a Bessel function, representing the free field that would exist in the absence of the jet. The scattered field is given by the Hankel function of the first kind, $H_m^{(1)}$. The constant $A_m(\omega, \theta)$ is then determined by matching the inner numerical solution to the far field sink, with the continuity of $\hat{G}_4$ and $d\hat{G}_4/dr$. The far field demarcation R_o, is physically defined as the the point where the mean flow has reduced to zero. Mathematically, it is chosen to be sufficiently large to allow the Bessel functions to approach their large argument asymptotic form. In this study we let $R_o = 20D_j$, where D_j is the nozzle exit diameter. The solution proceeds in a similar way for $\hat{G}_5$.

The second order equation, Eq. (40), requires that the derivatives of the mean flow, up to the second order $d^2\bar{M}/dr^2$, are adequately resolved. On the other hand, Eqs. (41) & (42) solve a conservation system that has eliminated all derivatives of the mean flow exactly. Hence, Eqs. (41) & (42) require the weaker condition of an adequately resolved mean flow, which is easily achieved in CFD solutions.

We restrict attention to a single azimuthal mode to investigate the behavior of the Green function, under the equation systems. The mean flow is based on the axial location of maximum source strength, i.e. the axial location where the amplitude of the source $q_s(\mathbf{y}, \omega)$ is maximum. For the Stromberg[4] case this is about $6D_j$ downstream of the nozzle. The mean velocity derivatives are computed using centered differences that are spatially filtered.[13] Fig. 1a shows the difference in predicted SPL at 30 degrees using the second order equation and the first order system. In this Figure, both systems use a mean flow profile defined with the

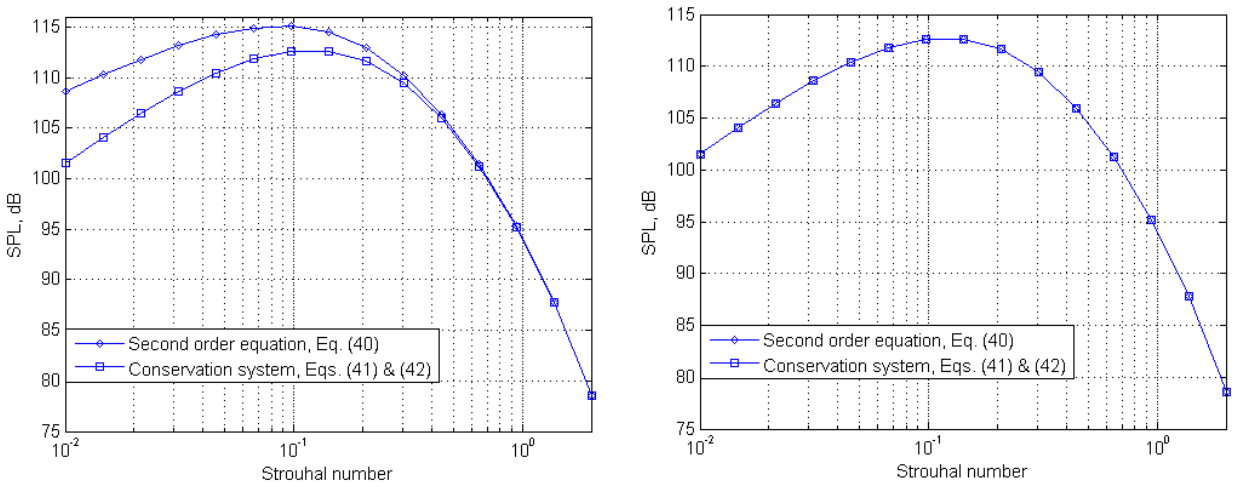

(a) Standard resolution mean flow: 88 nodes

(b) High resolution mean flow: 3000 nodes and spatial filtering

Figure 1. Sound Pressure Level, $SPL = 10\log(4\pi \mathbf{P}(\mathbf{x},\omega)/p^2_{ref}(D_j/U_j))$**, where** D_j **is the nozzle exit diameter;** U_j **is the nozzle exit velocity and** p^2_{ref} **is the reference pressure for Stromberg jet case.[4] Strouhal number,** $\omega D_j/2\pi U_j$ **based upon the nozzle exit diameter,** D_j**, and nozzle exit velocity,** U_j**. SPL predictions based on Green function with azimuthal mode = 0, observation angle** $= 30^o$**,** $\mid \mathbf{x} \mid = 30D_j$ **at the axial location of maximum source strength. Empirical coefficients,** (A, c_l, c_τ) **are** $(0.773, 0.130, 0.308)$ **taken from Morris and Farassat.[6]**

standard resolution of 88 points in the radial direction. The second order equation, Eq. (40), over predicts the SPL at low frequencies, compared to the first order system, Eqs. (41) & (42).

The low frequency sensitivity of the second order method can be corrected. We define the mean flow with enough resolution so that all derivatives of the mean flow, in the coefficients of Eq. (40), are adequately resolved. The resolution of the mean flow is increased uniformly, using quadratic interpolation defined with 3000 nodes. The mean flow is spatially filtered[13] and the derivatives are then computed using centered differences. Finally, these derivatives are spatially filtered[13] themselves. A thinner shear layer would, of course, require even greater resolution. See Fig. 1b.

The difference in SPL using the second order equation and the first order system emerges at the lowest frequencies and at the shallow observation angles (where the $\bar{D}_o = 1 + \bar{M}\hat{k}$ term has greater departures from unity). As the frequency increases the amplitude of the Green function is less affected by the high order derivatives of the mean flow compared to the variation of the mean flow itself. The second order equation remains accurate at high frequencies under standard resolution, because the Green function equations then degenerate to a form given by ray theory. The advantage of the solving the equations in a conservation form, without derivatives of the mean flow, is that they require less resolution. The subsequent noise predictions, for the parallel shear flow, use this convenient first order conservation system.

IV. Analysis of Far Field Noise

A. Ninety degree spectrum

In this section we compare the Tam and Aurialt model, Eq. (38), with various acoustic analogies, defined by Eq. (34). In these predictions the shear layer is based upon a mean flow at the axial location where the source amplitude is maximum. Fig. 2 shows the ninety degree spectrum with comparison to the Tanna jet case[6] .

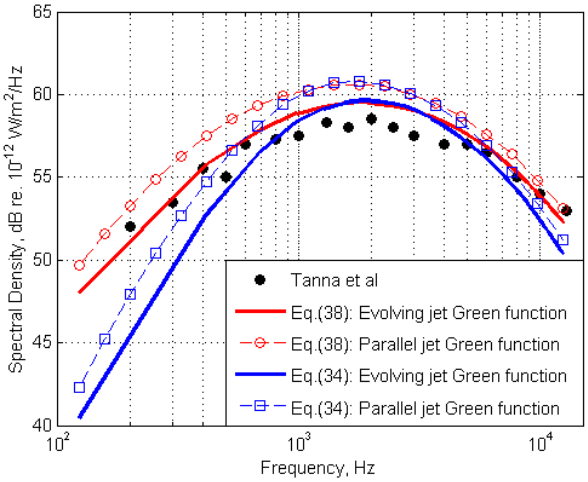

Figure 2. Sound Pressure Level, $SPL = 10\log(4\pi \mathbf{P}(\mathbf{x},\omega)/p^2_{ref}(D_j/U_j))$, where D_j is the nozzle exit diameter; U_j is the nozzle exit velocity and p^2_{ref} is the reference pressure. Parallel jet Green function using Eqs. (41) & (42) based on the axial location of maximum source strength. Evolving jet Green function from Karabasov and Hynes.[12] Empirical coefficients for Eq. (34), (A, c_l, c_τ) are $(0.125, 0.45, 0.125)$; Eq. (38), (A, c_l, c_τ) are $(0.773, 0.130, 0.308)$.[6] The experimental results from Tanna *et al* given by Morris and Farassat.[6]

If we compare acoustic analogy predictions to the Tam and Aurialt model, we find although they both have similar maximum sound intensity, the acoustic analogies have steeper decay at high and low frequencies. This arises because the acoustic analogy has the ω^4 factor in the spectrum, compared to the ω^2 and characteristic time scale factor, $1/\tau_s^2$, for the Tam and Aurialt model. This is summarized in Table 1.

Table 1. Comparison of Acoustic analogy and Tam and Aurialt.

Model	Green function	Source function	90^o Frequency scaling
Acoustic analogy Eq. (34)	$\left\vert \frac{D_1 \hat{G}_4}{D\tau}(\mathbf{y},\omega \mid \mathbf{x}) \right\vert^2$	$q_s(\mathbf{y},\omega)$	ω^4
Tam and Aurialt Eq. (38)	$\mid \hat{G}_4(\mathbf{y},\omega \mid \mathbf{x}) \mid^2$	$q_s(\mathbf{y},\omega)/\tau_s^2$	ω^2

B. Sensitivity to the Radial Location of Maximum Shear

We have shown how a representation that uses $\hat{G}_4$, and assumes a model form for the convective derivative of the source, can result in a power spectral density defined by a discontinuous integrand: Eq. (38). In this section we assess the behavior of Eq. (38) by choosing different mean flow profiles as the basis for the Green function product, $\mid \hat{G}_4 \mid^2$. Comparison is made to Eq. (34), which defines a power spectral density using the convective derivative of the Green function, $D_1\hat{G}_4/D\tau$.

For a vortex sheet type mean flow we position the sheet along the jet boundary, at the radial location of maximum shear (max $\mid dU/dr \mid$) for a particular mean velocity profile. We displace the vortex sheet relative to the source position, by choosing different mean flow profiles to base the Green function on. The sensitivity of the sound pressure can then be assessed for the vortex sheet, and parallel shear layer, using the power spectral density equations, Eqs. (34) and (38). This is shown in Figs. 3a and 3b for the vortex sheet Green function at 30 and 60 degrees. The Strouhal number, $\omega D_j/2\pi U_j$; based upon the nozzle exit diameter, D_j,

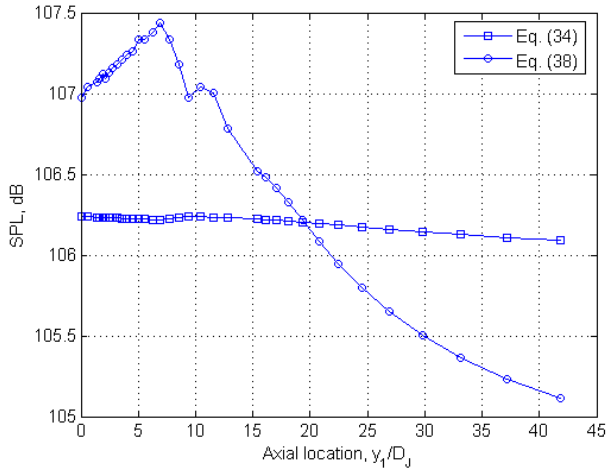

(a) Vortex Sheet, 30 degrees

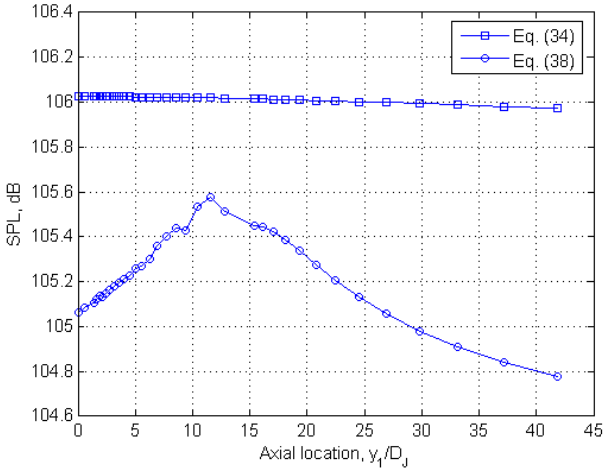

(b) Vortex Sheet, 60 degrees

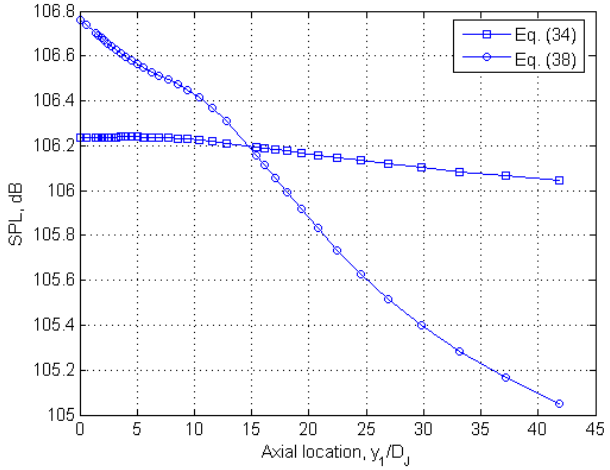

(c) Shear layer, 30 degrees

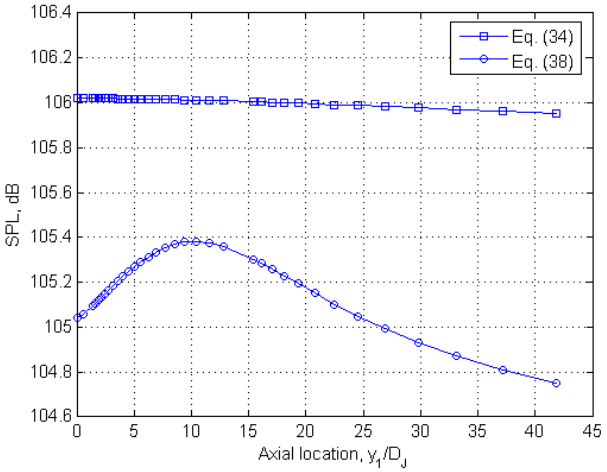

(d) Shear layer, 60 degrees

Figure 3. Sound Pressure Level variation. D_j **is the nozzle exit diameter and** y_1 **is the axial location in the jet direction.** $SPL = 10\log(4\pi \mathbf{P}(\mathbf{x},\omega)/p^2_{ref}(D_j/U_j))$**; where,** U_j **is the nozzle exit velocity;** $\mid \mathbf{x} \mid = 30D_j$**;** p^2_{ref} **is the reference pressure for Stromberg jet case[4] and** $\mathbf{P}(\mathbf{x},\omega)$ **is determined using a Green function placed at various axial locations,** y_1**. Strouhal number,** $\omega D_j/2\pi U_j$**, is 0.02. Azimuthal mode,** $m = 0$**. Empirical coefficients for Eq. (34) and Eq. (38),** (A, c_l, c_τ) **are** $(0.773, 0.130, 0.308)$**[6]**

and nozzle exit velocity, U_j, is 0.02 for the Stromberg jet. Figs. 3c and 3d show the sensitivity in predicted sound power for the parallel shear flow, defined by the same observation angles and frequency.

Sound predictions using Eq. (38), results in an integrand that is discontinuous across a vortex sheet; and varies significantly across a shear layer. This leads to the predicted sound being sensitive to the position of the turbulent sources relative to the mean velocity profile. On the other hand Eq. (34), which uses the conserved quantity $D_1\hat{G}_4/D\tau$, displays only little sensitivity to the mean velocity profile chosen to define the parallel jet. Once the radial length scale over which the mean flow profile varies is comparable with the acoustic wavelength, we begin to see acoustic propagation effects dependent on the mean flow profile.

V. Conclusions

We have investigated various acoustic analogies and found the representation theorem of Goldstein[7] is particularly advantageous. In the course of this, we have reanalyzed the Tam and Aurialt formulation, which Morris and Farassat[6] have shown is equivalent to an acoustic analogy where, $D_1 T_{ij}/D\tau$ is modeled with Gaussian statistics. In addition to the frequency scaling problem this raises, i.e. $T_{ij} \to \infty$ as $\omega \to 0$,[6,7] there is another problem because the equivalent Green's function (G_4 in our notation: G_4 being the independent variable in the adjoint energy equation defined by Eq. (14)) is discontinuous across a vortex sheet and rapidly varying across a shear layer. This leads to sensitivity of the predicted sound (provided θ not equal to 90 degrees) to the details of the mean velocity profile.

There will always be some ambiguity in the choice of the mean flow velocity, if an evolving jet is represented by a parallel shear flow. The acoustic analogy leads to an integrand proportional to $D_1 G_4/D\tau$, in Eq. (34). This term is continuous across a vortex sheet and varies insignificantly across a thin shear layer. It leads to a predicted sound field that is *remarkably* insensitive to uncertainties in the mean flow profile.

We have found it convenient to solve the propagation equations for $G_5 \sim D_1 G_4/D\tau$. It is then possible to cast the parallel flow propagation equations in a conservation form which involves no mean flow derivatives. This has a particular advantage when the mean flow is determined from a near field CFD calculation, and known only at discrete points that may have small oscillations. In this paper we have concentrated on propagation effects seen through the Green's function using a simple source description. Future work will involve more accurate modeling of the source. Our current assumption of isotropic turbulence and Gaussian statistics is clearly an oversimplification. We aim to use LES data to model the statistics of the large-scale structures, and improved turbulence models for the small-scale.

Acknowledgments

This work is part of a collaborative project on jet noise funded by the Engineering and Physical Sciences Research Council (EPSRC) whose support is gratefully acknowledged. We are grateful for helpful discussions with colleagues at the Universities of Cambridge and Loughborough and Rolls-Royce, particularly Dr Tom Hynes, Professor Jim McGuirk, Drs Gary Page and Jason Wu, who provided the CFD data.

References

[1]Lighthill, M. J., "On Sound Generated Aerodynamically: I. General Theory," *Proceedings of the Royal Society of London, A:*, Vol. 222, 1952, pp. 564–587.

[2]Lilley, G. M., "On the Noise from Jets," *CP-131 AGARD*, 1974, pp. 13.1–13.12.

[3]Freund, J. B., "Noise source Turbulence statistics and the Noise from a Mach 0.9 Jet," *Physics of Fluids*, Vol. 15, No. 6, 2003, pp. 1788–1800.

[4]Stromberg, J. L., McLaughlin, D. K., and Troutt, T. R., "Flow Field and Acoustic Properties of a Mach Number 0.9 Jet at a Low Reynolds Number," *Journal of Sound and Vibration*, Vol. 72, No. 2, 1980, pp. 159–176.

[5]Tam, C. K. W. and Aurialt, L., "Jet Mixing Noise from Fine Scale Turbulence," *AIAA Journal*, Vol. 206, No. 2, 1999, pp. 145–153.

[6]Morris, P. J. and Farassat, F., "Acoustic Analogy and Alternative Theories for Jet Noise Prediction," *AIAA Journal*, Vol. 40, No. 4, 2002, pp. 671–680.

[7]Goldstien, M. E., "Ninety-Degree Acoustic Spectrum of a High-Speed Air Jet," *AIAA Journal*, Vol. 43, No. 1, 2005, pp. 96–102.

[8]Goldstein, M. E., "A unified approach to some recent developments in jet noise theory," *Journal of Aeroacoustics*, Vol. 1, No. 1, 2002, pp. 1–16.

[9]Dowling, A. P., Ffowcs-Williams, J. E., and Goldstein, M. E., "Sound Production in a moving stream," *Proceedings of the Royal Society of London, Series A: Mathematical and Physical Sciences*, Vol. 288, 1978, pp. 321–349.

[10]Tam, C. K. W. and Aurialt, L., "Mean flow refraction effects on sound radiated from localized sources in a jet," *Journal of Fluid Mechanics*, Vol. 370, 1998, pp. 149–174.

[11]Agarwal, A., Morris, P. J., and Mani, R., "Sound Propagation in Non-uniform flows: Suppression of instability waves," *AIAA Journal*, Vol. 42, No. 1, 2004, pp. 80–88.

[12]Karabasov, S. A. and Hynes, T. P., "Adjoint linearized Euler solver in the frequency domain for Jet Noise Modeling," *12th AIAA/CEAS, Cambridge, Massachusetts*, 2006.

[13]Vasilyev, O. V., Lund, T. S., and Moin, P., "A General Class of Commutative Filters for LES in Complex Geometries," *Journal of Computational Physics*, Vol. 146, 1998, pp. 82–104.